

# 11-2 A New Quasi Ballistic Model for Strained MOSFET.

E.Fuchs<sup>1,2,3</sup>, S. Orain<sup>4</sup>, C. Ortolland<sup>4</sup>, P. Dollfus<sup>2</sup>, G. Le Carval<sup>3</sup>, D. Villanueva<sup>4</sup>, A.Dray<sup>1</sup>, H. Jaouen<sup>1</sup>, T. Skotnicki<sup>1</sup>.  
<sup>1</sup>ST Microelectronics, <sup>4</sup>Philips Semiconductor, Crolles, France.  
<sup>2</sup>IEF, CNRS-University Paris 11, Orsay, France. <sup>3</sup>CEA LETI/D2NT/LSCDP Grenoble, France.  
 E-mail: [emmanuel.fuchs@st.com](mailto:emmanuel.fuchs@st.com), Phone: +33 4 76 92 26 75.

**Abstract** - An analytical model for the nano-MOSFET based on the determination of ballistic and backscattering probabilities along the channel is developed. This model, validated by analysis of transport in device using scattering spectroscopy, has been used to model the strained MOSFET by evaluating the appropriate scattering relaxation times and the carrier distribution. Finally, it has been used to determine the impact of CESL on the  $I_{ON}$  enhancement.

## I-INTRODUCTION

Recent works showed that the local strain generated in Si using technology process steps is a promising way to improve the  $I_{ON}/I_{OFF}$  trade-off [1]. The strain distribution can be computed using finite elements simulation [2]. We propose here a general compact model to study the stress impact on I(V) characteristics. The Bir-Pikus theory is used to calculate the valley splitting in Si as a function of local strain [3]. The scattering relaxation times and the carrier distribution are deduced. From these new inputs, an accurate determination of ballistic and backscattering probabilities along the channel is used to compute the backscattering coefficient and the I(V) characteristic as explained in [4]. This model is validated by scattering spectroscopy resulting from Monte Carlo (MC) simulation for a Si/Si<sub>0.7</sub>Ge<sub>0.3</sub> MOSFET and it is used to study the effects of Strained Contact Etch Stop Layer (CESL) on 65 nm MOS transistor performance.

## II-ANALYTICAL QUASI BALLISTIC MODEL

The model developed in [5] allows determining the backscattering coefficient  $R_C$  and the injection velocity to calculate the current  $I_{DS}$ :

$$I_{DS} (V_{DS} \gg kT) = C_{ox} W (V_G - V_{th}) \times v_{therm} \frac{1 - R_C}{1 + R_C} \quad (1)$$

To determine  $R_C$ , the first step consists in determining the potential profile at  $V_{DS}$  and  $V_{GS}$ , which is done from evaluation of the saturation drain voltage and the length of the pinch off zone by taking into account the access resistance as illustrated in Figure 1. The expression used for the potential was validated in [4].

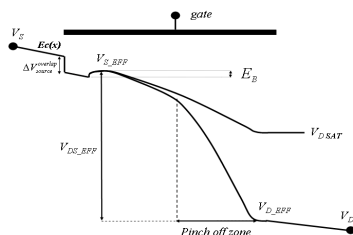


Figure 1: Illustration of the potential profile

Secondly, we compute the average thermal velocity from the conduction effective mass taking into account the carrier distribution  $P_X, P_Y, P_Z$  in the different types of  $\Delta$  valleys:

$$v_{therm} = \sqrt{\frac{2kT}{\pi m_c^*}} = \sqrt{\frac{2kT}{\pi} \left( \frac{P_X}{m_X} + \frac{P_Y}{m_Y} + \frac{P_Z}{m_Z} \right)} \quad (2)$$

Then, from the scattering relaxation times and the velocity of ballistic carriers we obtain the ballistic probabilities  $N_{bal-i}(x)$  (Fig. 2) along the channel as:

$$N_{bal-i}(x + dx) = N_{bal-i}(x) \exp\left(-\frac{dx}{\tau_{tot-i}(x) \cdot v_{bal-i}(x)}\right) \quad (3)$$

For different drain and gate voltages, the model is validated for the MOSFET described in [6] (Figure 2).

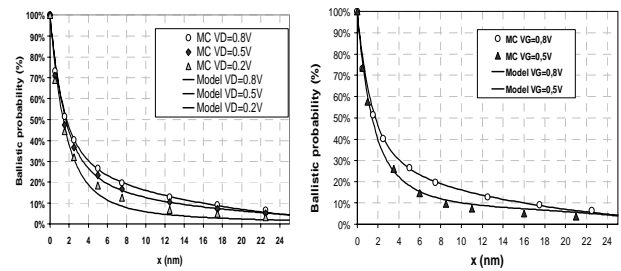


Figure 2: Ballistic probabilities  $N_{bal-i}(x)$  at  $V_{GS}=0.8V$  (right) and at  $V_{DS}=0.8V$  (left) MOSFET  $L_{ch}=25nm$   $N_{ch}=5.710 \cdot 10^{18} cm^{-3}$   $t_{ox}=1.2nm$

From the probability  $N_{bal-i}(x)$  we can deduce the probability  $N_{scat-it}(x)$  for an electron to have its first scattering event at position  $x$ :

$$N_{scat-i}(x + dx) = N_{bal-i}(x) - N_{bal-i}(x + dx) \quad (4)$$

Then, we determine the backscattering probabilities  $P_{RC}(x)$  for a ballistic carrier of the valley  $i$  having a scattering event at  $x$  to be sent back to the source with (5) as explained in [4].

$$P_{RC}(x) = \frac{T_S(x)}{T_S(x) + T_D(x)} \quad (5)$$

This probability of backscattering is illustrated in Figure 3:

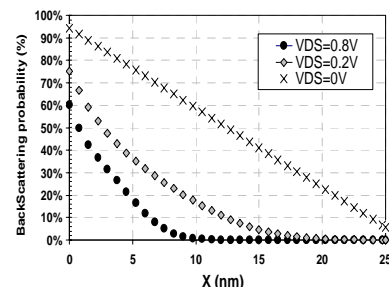


Figure 3: Backscattering probabilities  $P_{RC}(x)$  at  $V_{GS}=0.8V$

These probabilities are integrated over the entire channel to obtain the fraction of backscattering  $F_{RC-i}(x)$ :

$$F_{RC}^i(x) = \int_0^x P_{RC}(x) N_{scat}^i(x) dx \quad (6)$$

and the coefficient  $R_C$  is deduced by taking into account the carrier distribution as illustrated in Figure 4:

$$F_{RC}(x) = P_X F_{RC}^X(x) + P_Y F_{RC}^Y(x) + P_Z F_{RC}^Z(x) \quad (7)$$

And

$$R_c = F_{RC}(L_{ch}) \quad (8)$$

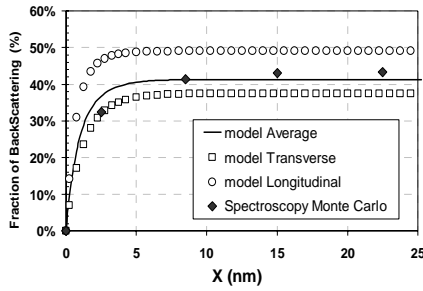


Figure 4: Fraction of backscattering probabilities  $F_{RC-i}(x)$  at  $V_{GS}=0.8V$  and  $V_{DS}=0.8V$  for the MOSFET  $L_{ch}=25nm$

This backscattering model can correctly reproduce the universal mobility based on the Takagi data [6]. Finally, thanks to 2 fitting parameters for the description of short channel effects, the charge at the top of the barrier is computed and the I(V) characteristics are modelled and validated by Monte Carlo simulation as illustrated in Figure 5. This result shows that the model is able to describe continuously the different regimes of transport, from purely stationary to purely ballistic.

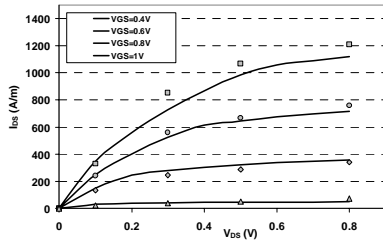


Figure 5: I(V) characteristic for the MOSFET  $L_{ch}=25nm$

### III-VALIDATION ON $Si_{0.7}Ge_{0.3}$ MOSFET

Considering an arbitrary stress  $(S_{XX}, S_{YY}, S_{ZZ})$ , the crystal deformations are obtained with the Young modulus  $E$  and Poisson's ratio  $\nu$  and the deformation potentials  $(\Xi_d, \Xi_u)$ . These deformations are introduced in the Bir-Pikus equations [4]:

$$\begin{aligned} \epsilon_{XX} &= \frac{S_{XX}}{E} - \frac{\nu}{E}(S_{YY} + S_{ZZ}) \\ \Delta E_{C-X} &= \Xi_d(\epsilon_{XX} + \epsilon_{YY} + \epsilon_{ZZ}) + \Xi_u \epsilon_{XX} \\ \Delta E_{C-Y} &= \Xi_d(\epsilon_{XX} + \epsilon_{YY} + \epsilon_{ZZ}) + \Xi_u \epsilon_{YY} \\ \Delta E_{C-Z} &= \Xi_d(\epsilon_{XX} + \epsilon_{YY} + \epsilon_{ZZ}) + \Xi_u \epsilon_{ZZ} \end{aligned} \quad (9)$$

which allows computing the shifts of energy in the conduction band  $\Delta E_{C-X}$ ,  $\Delta E_{C-Y}$ ,  $\Delta E_{C-Z}$  and in the valence band  $\Delta E_{V-hh}$ ,  $\Delta E_{V-lh}$  as illustrated in Figure 6.

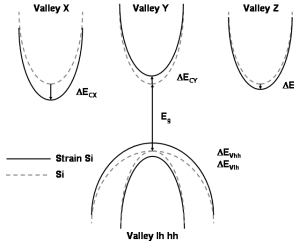


Figure 6: New band structure under an unspecified stress

With this new band structure, the intrinsic carrier concentration is calculated by averaging the contributions of the different bands using (10) to determine the new threshold voltage.

$$n_i^2 = \sum_{\substack{i=X,Y,Z \\ j=hh,lh}} N_{C-i} N_{V-j} \exp\left[-(E_g + \Delta E_{C-i} - \Delta E_{V-j})/kT\right] \quad (10)$$

Then, the new carrier distribution is calculated using the probabilities to have an electron in the valley  $i$  given by:

$$P_i = \frac{e^{-\Delta E_{C-i}/kT}}{\sum_{i=X,Y,Z} e^{-\Delta E_{C-i}/kT}} \quad (11)$$

From these probabilities we determine the conduction effective mass  $m_C^*$  and the thermal velocity is calculated using (2). Then, for each valley  $i$ , the ballistic velocity and the scattering relaxation times are determined to compute the ballistic probabilities with (4). In this paper, the previous MOSFET is studied and compared with similar biaxial tensile  $Si/Si_{0.7}Ge_{0.3}$  MOSFETs. Most carriers are in the lowest transverse valley Z and their probabilities to have an intervalley scattering towards the other valleys are weak. Consequently, there are more ballistic carriers than in unstrained MOSFET as illustrated in Figure 7 and Figure 8.

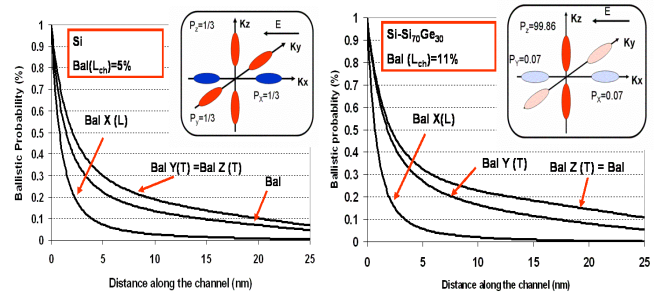


Figure 7: Ballistic probabilities for a Si-MOSFET and a biaxial tensile  $Si_{0.7}Ge_{0.3}$  MOSFET at  $V_{DS}=V_{GS}=0.8V$ . (model curves)

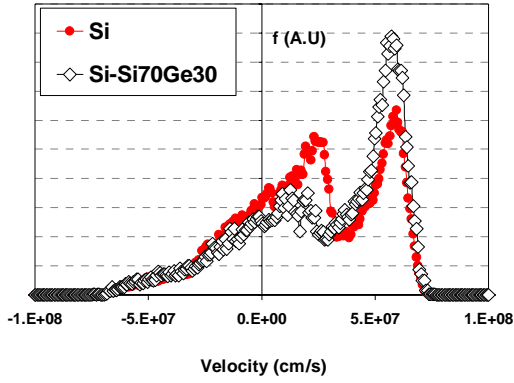


Figure 8: Distribution function for a Si-MOSFET and a biaxial tensile Si<sub>0.7</sub>Ge<sub>0.3</sub> MOSFET at  $V_{DS}=V_{GS}=0.8V$   $L_{ch}=25nm$

The next step consists in computing the backscattering probabilities along the channel for each type of valley with the mean free path  $mfp = v_{th} x < \tau >$  and the repulsive source field and attractive drain field [3]. The global backscattering probabilities (Fig. 8) and the backscattering coefficient  $R_C$  are then computed. Finally, taking into account the carrier distribution at the top of the barrier, we obtain the fraction of backscattering plotted on Figure 9.

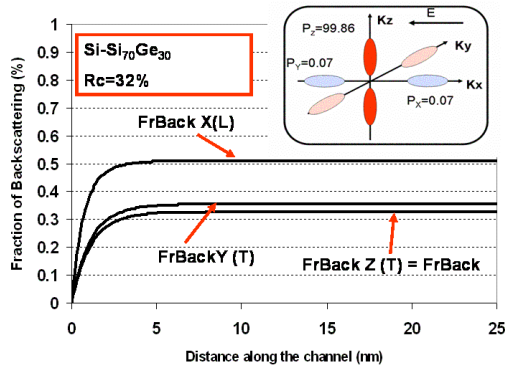


Figure 9: Fraction of backscattering for a Si-MOSFET and a biaxial tensile Si<sub>0.7</sub>Ge<sub>0.3</sub> MOSFET at  $V_{DS}=V_{GS}=0.8V$

The I(V) characteristics are in good agreement with Monte Carlo simulation as illustrated in Figure 10.

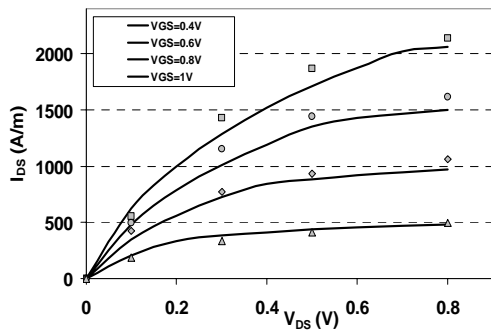


Figure 10: I(V) characteristic for a Si-MOSFET and a biaxial tensile Si<sub>0.7</sub>Ge<sub>0.3</sub> MOSFET  $L_{ch}=25nm$

We define the current gain in strained device as the ratio of  $I_{on}$  to the value of  $I_{on}$  obtained in unstrained MOSFET. To verify the field dependence on the gain enhancement, the gain versus

$L_G$  on different MOSFETs plotted and validated on Figure 11 called the “S curve”

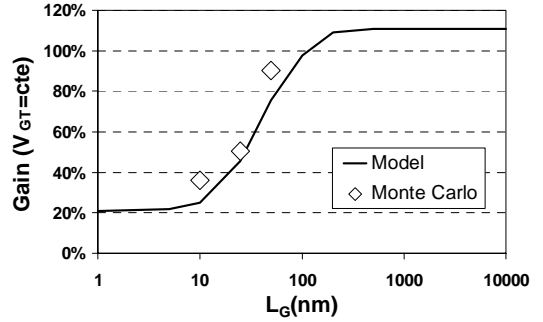


Figure 11: Comparisons of the current gain between our model and Monte Carlo simulation at  $V_{DS}=V_{GS}=0.8V$ .

When  $L_G$  decreases, the field increases and the carrier gas energy is larger than the maximum shift  $\Delta E_{C-i}$ . So, the distribution in the valleys at high field is close to the equilibrium distribution:  $P_x=P_y=P_z=1/3$  and the current gain decreases. The limit cases are the following. In the diffusion case the gain is due to the scattering relaxation time and the effective conductive mass (Figure 12).

$$Diffusion \Rightarrow \frac{\Delta I_{DS}}{I_{DS}} \Big|_{I_{OFF}=cte} = \frac{\Delta \mu}{\mu} = \frac{\Delta \langle \tau \rangle}{\langle \tau \rangle} + \frac{\Delta m_c^*}{m_c^*} \quad (12)$$

And in the ballistic case, the gain is due to the thermal velocity. It explains the saturation at small channel length (Figure 12):

$$Ballistic (R_C = 0) \Rightarrow \frac{\Delta I_{DS}}{I_{DS}} \Big|_{I_{OFF}=cte} = \frac{\Delta v_{therm}}{v_{therm}} = \frac{1}{2} \frac{\Delta m_c^*}{m_c^*} \quad (13)$$

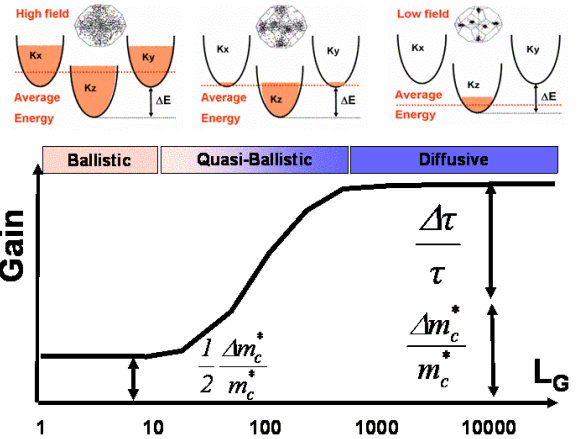


Figure 12: “S curve” illustration with the limit cases.

#### IV-APPLICATION on CESL C65 MOSFET

The CESL is the first layer above the transistor, so it can easily transmit its intrinsic strain on the channel. To further understand the electrical phenomena, ANSYS 3D elastic simulations have been performed to determine the relative contribution of the CESL to the stress in the channel [2] as describes in Figure 13.

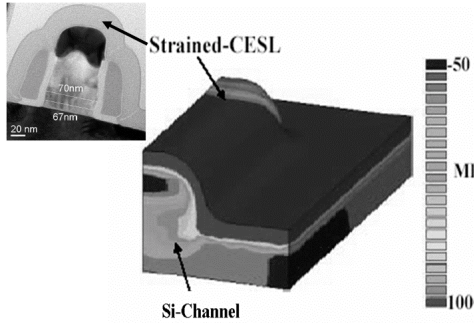


Figure 13: 3D schematic view of the stress due to the tensile CESL (1GPa) in a 1/4 MOS. Materials are stress free except CESL.

For C65 MOS transistors technology with a tensile CESL of 50nm as described in [2], stress components ( $S_{XX}$ ,  $S_{YY}$ ,  $S_{ZZ}$ ) versus  $L_G$  are plotted on Figure 14

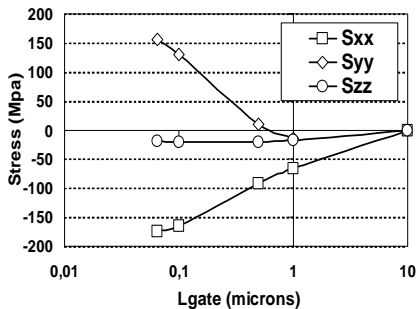


Figure 14: Mechanical simulation data for a CESL tensile 50nm. X: transport direction, Z: Gate Stack direction.

With these inputs the new  $V_{th}$  and currents are computed using our model. For tensile stresses resulting from 50nm and 30nm CESL, a correct agreement between experimental and modeling data is found for the threshold voltage variation as illustrated on Figure 15.

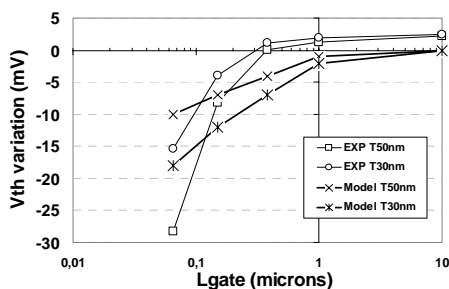


Figure 15: Threshold voltage variation versus  $L_G$ . Comparisons between experimental data and the new model.

and for the current enhancement on the Figure 16.

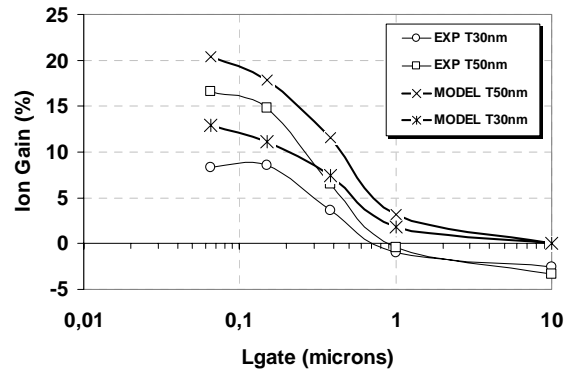


Figure 16:  $I_{ON}$  enhancement versus  $L_G$ . Comparisons between experimental data and our new model.

This agreement is obtained despite the numerous approximations made in the model used for mechanical process and device simulations. Additionally, it should be mentioned that the possible initial stress existing in the real devices is not included in the simulation, which may explain the slight discrepancy between experimental and simulation results.

#### V- CONCLUSION

Based on carrier spectroscopy from Monte Carlo simulations, we have developed a new efficient and rigorous backscattering model including an arbitrary strain. Validated for different  $Si_{0.7}Ge_{0.3}$  MOSFET this model allows visualizing the main effects of the stress on carrier transport along the channel. Finally, this model can be used to predict  $I_{ON} / I_{OFF}$  trade-off improvement by using the results of relevant process mechanical simulations.

#### VI- REFERENCES

- [1] C.T. Huang, "A novel Local Strain Scheme with Strong 45nm CMOS Performance for Broad Applications", IEDM 2004.
- [2] C.Ortolland, "Electrical Characterization and Mechanical Modelling of Process Induced Strain in 65 nm CMOS Technology", ESSEDERC 2004, p. 137-140.
- [3] G.L. Bir, G.E. Pikus, "Symmetry and Strain-induced Effects in Semiconductors, Wiley, 1972.
- [4] E.Fuchs "A New Backscattering Model giving a Description of the Quasi Ballistic Transport", submitted to IEEE TED
- [5] M.S. Lundstrom, "A Landauer Approach to Nanoscale MOSFETs", Journal of Computational Electronics, vol. 1, pp. 481-489, 2002.
- [6] E. Fuchs, P. Dollfus, G. Le Carval, S. Barraud, D. Villanueva, F. Salvetti, H. Jaouen, T. Skotnicki, "A New Backscattering model for Nano MOSFET", SNW VLSI, 2005.